

Strain-driven onset of nontrivial topological insulating states in Zintl Sr_2X compounds ($X = \text{Pb, Sn}$)Yan Sun,¹ Xing-Qiu Chen,^{1,*} Cesare Franchini,^{1,2} Dianzhong Li,¹ Seiji Yunoki,³ Yiyi Li,¹ and Zhong Fang⁴¹Shenyang National Laboratory for Materials Science, Institute of Metal Research, Chinese Academy of Sciences, Shenyang 110016, China²Center for Computational Materials Science, University of Vienna, Sensengasse 8, A-1090 Vienna, Austria³Computational Condensed Matter Physics Laboratory, RIKEN ASI, Saitama 351-0198, Japan; CREST, Japan Science and Technology Agency (JST), Saitama 332-0012, Japan; and Computational Materials Science Research Team, RIKEN AICS, Hyogo 650-0047, Japan⁴Beijing National Laboratory for Condensed Matter Physics, Institute of Physics, Chinese Academy of Sciences, Beijing, 100081, China

(Received 30 September 2011; published 25 October 2011)

We explore the topological behavior of the binary Zintl phase of the alkaline-earth-metal-based compounds Sr_2Pb and Sr_2Sn using both standard and hybrid density functional theory. It is found that Sr_2Pb lies on the verge of a topological instability which can be suitably tuned through the application of a small uniaxial expansion strain ($>3\%$). The resulting nontrivial topologically insulating state displays well-defined metallic states in the $\text{Sr}_2\text{Pb}(010)$ surface, whose evolution is studied as a function of the film thickness.

DOI: 10.1103/PhysRevB.84.165127

PACS number(s): 71.20.-b, 73.20.-r, 73.43.-f

I. INTRODUCTION

Topological insulators¹⁻⁶ (TIs) are a new quantum state of matter characterized by the existence of gapless surface states sheltered against destructive scattering effects by time-reversal symmetry. Since the discovery of two-dimensional TI behaviors of HgTe-based quantum wells,^{7,8} several families of topological materials have been theoretically predicted and experimentally realized.^{1,9} The variety of insulating materials displaying topological features includes $\text{Bi}_x\text{Sb}_{1-x}$ alloys,^{5,10} Bi_2Te_3 , Bi_2Se_3 , and Sb_2Te_3 binary compounds,^{6,9,11-13} ternary heavy-metal-based compounds such as TlBiTe_2 , TlBiSe_2 ,¹⁴⁻¹⁶ and PbBi_2Se_4 ,^{17,18} ternary rare-earth chalcogenides (LaBiTe_3),¹⁹ and another honeycomb-lattice type of ternary compounds (LiAuSe).²⁰ All these materials are characterized by a layered structure stacked along the c axis of the centrosymmetric hexagonal lattice, similar to the structure of Bi_2Se_3 . In addition, other ternary TIs have been recently predicted such as the noncentrosymmetric cubic zinc-blende HgTe-like phase (half-Heusler compounds²¹⁻²³ and I-III-VI₂ and II-IV-V₂ chalcopyrite semiconductors such as AuTlTe_2 ^{24,25}) and Ca_3NBi with a centrosymmetric antiperovskite structure.²⁶ Although a large number of ternary TIs have been found,^{14-19,21-25} up to now, binary TIs are limited to only three classes: $\text{Bi}_{1-x}\text{Sb}_x$ alloys and the family of Bi_2Te_3 , Bi_2Se_3 , and Sb_2Te_3 as well as Ag_2Te .²⁷ In the present paper we investigate the possible realization of topological behaviors in binary semiconductors. In searching for new TI materials we have focused our attention on binary heavy-element-based small-band-gap semiconductors. One of the simplest ways to realize a binary heavy-element-based closed-shell semiconductor is to have M_2X with an alkaline earth element ($M = \text{Mg, Ca, Sr, and Ba}$) which donates its s valence electron to a group IV element ($X = \text{Si, Ge, Sn, and Pb}$). These are the so-called Zintl compounds.

The Zintl compounds M_2X crystallize in a simple orthorhombic crystal structure,^{28,29} as illustrated in Fig. 1. The X atoms surround the M atoms in a slightly distorted trigonal-prismatic coordination. The coordination sphere is augmented by the three X atoms situated on the rectangular faces of these prisms (tricapped trigonal prism). Along the a direction the prisms are condensed via common edges while

they share common triangular faces along the b direction. The semiconducting character of these compounds originates from their closed-shell nature, with six valence electrons ($2 \times s^2 + p^2$) per formula unit [$(2M^{2+})X^{4-}$].

In the following we first describe our computational methodology and then we present and discuss the bulk and surface results.

II. COMPUTATIONAL ASPECTS

We have performed band-structure calculations using the Perdew-Burke-Ernzerhof³⁰ (PBE)-based standard and hybrid Heyd-Scuseria-Ernzerhof³¹ (HSE) density functional theory (DFT) as implemented in the Vienna Ab initio Simulation Package (VASP),^{32,33} employing the projected augmented wave approach and including relativistic spin-orbit coupling (SOC) effects, for all bulk and surface calculations. Within the HSE method, the many-body exchange and correlation functional is constructed by mixing 25% exact Hartree-Fock exchange with 75% PBE, and the long-range Coulomb interaction is suitably screened according to the parameter μ (here $\mu = 0.3 \text{ \AA}^{-1}$).³¹

We have employed the experimental lattice constants and relaxed (in the bulk) all atomic positions with a force tolerance of 0.001 eV/\AA , adopting a standard convergence criteria for the electronic self-consistent loop (10^{-4} eV), and using a very dense k -point mesh (up to 4200 k points) and an energy cutoff of 500 eV.

In the surface calculations we have used a symmetric slab approach including up to 100 bulk unit cells (u.c.), resulting in an extremely large supercell containing up to 1200 atoms. Due to the increased computational cost, slab calculations were done only at the PBE level, using a reduced energy cutoff of 250 eV and, for slab thickness larger than 34 u.c., only the Γ point was included in the k -space integration.

III. RESULTS AND DISCUSSION

Our preliminary PBE-based research of possible topological features in this class of materials revealed that two members of the Zintl family (Sr_2Pb and Ba_2Pb) exhibit promising fingerprints of TI behaviors, whereas the remaining compounds are either trivial insulators (Ca_2Ge , Sr_2Ge , Ca_2Sn , and Sr_2Sn)

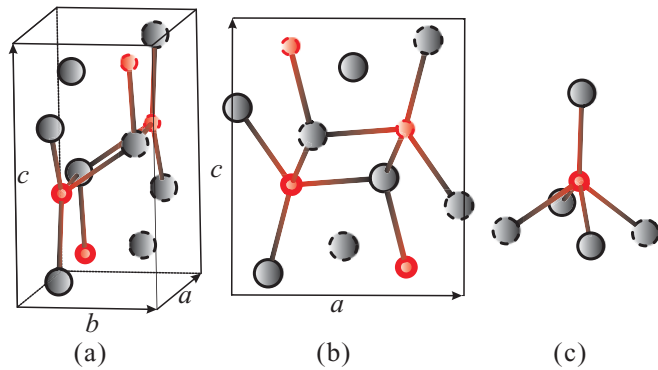


FIG. 1. (Color online) Structure representations of orthorhombic (space group $Pnma$, No. 62) M_2X compounds ($M = \text{Mg, Ca, Sr, Ba}$; $X = \text{Si, Ge, Sn, Pb}$): (a) the unit cell, (b) the projection of the unit cell in the ac plane, perpendicular to the b axis, and (c) the local environment around the X atom. The large (gray) and small (red) balls denote the M and X atoms, respectively. In addition, along the b axis ($y = 1/4$ and $y = 3/4$) the atoms can be arranged in two parallel planes shown in the dashed and solid balls, respectively. M occupies two inequivalent $4c$ sites, M_1 ($x_1, 1/4, z_1$) and M_2 ($x_2, 1/4, z_2$), whereas X occupies the $4c$ site ($x_3, 1/4, z_3$). For Sr_2Pb the optimized atomic positions are Sr_1 (0.0214, 1/4, 0.683), Sr_2 (0.1580, 1/4, 0.073), and Pb (0.2496, 1/4, 0.3929).

or semimetal (Ba_2Ge , Ca_2Pb , and Ba_2Sn). Therefore in the following we focus our analysis on these two specific Zintl compounds: Sr_2Pb and Sr_2Sn .

The DFT band structures with and without SOC effects are compared in Figs. 2(a)–2(d). The inclusion of SOC effects does not affect the overall electronic character of Sr_2Sn [Figs. 2(a) and 2(b)], which remains a semiconductor with a small band gap at Γ (≈ 0.15 eV) opened between occupied Sn p_x states

and highly dispersive Sr d -like empty orbitals (mostly $d_{x^2-y^2}$). By replacing Sn with the isoelectronic heavier element Pb, the band structure changes dramatically, as schematically depicted in Fig. 3(a). Without SOC, Sr_2Pb displays a metallic (gapless) state [Fig. 2(c)], whereas the inclusion of SOC [Fig. 2(d)] opens a band gap of about 100 meV at Γ (the indirect gap is about 50 meV), as a consequence of the anticrossing between the conduction band minimum and valence band maximum (VBM), a typical fingerprint of the SOC-induced formation of topological insulating states. The major differences between the electronic structure of Sr_2Sn and Sr_2Pb resides in the orbital character of the valence and conduction bands near Γ as highlighted by the (red) solid circles in the band plot of Figs. 2(a)–2(d): in Sr_2Sn the states with a predominant s -like character lie about 0.5 eV above the Fermi level [see Figs. 2(a) and 2(b)], whereas in Sr_2Pb these states are pushed down in energy and eventually hybridize the VBM at Γ , thus inducing the anticrossing feature responsible for the opening of the gap and the creation of a TI state. The downward shift of the s states is accompanied by an upward shift of the heavy-metal p bands which ultimately intermix with the Sr d states as schematized in Fig. 3(a).

As recently reported by Zunger and coworkers,³⁴ the identification of band-inverted TI^{7,8} on the basis of conventional DFT may lead to false-positive assignment if the band-inversion strength is not large enough, due to the well-documented band-gap underestimation problem. For this reason we have revisited the electronic dispersion of Sr_2Pb by HSE, which indeed yields a substantially different physical picture, as illustrated in Figs. 2(e) and 2(f). HSE finds a much larger band gap (0.25 eV), which is reduced to 0.13 eV with the inclusion of SOC effects and, most importantly, prevents the occurrence of band inversion between the p_x -like and s -like states as schematically illustrated in Fig. 3(b). The

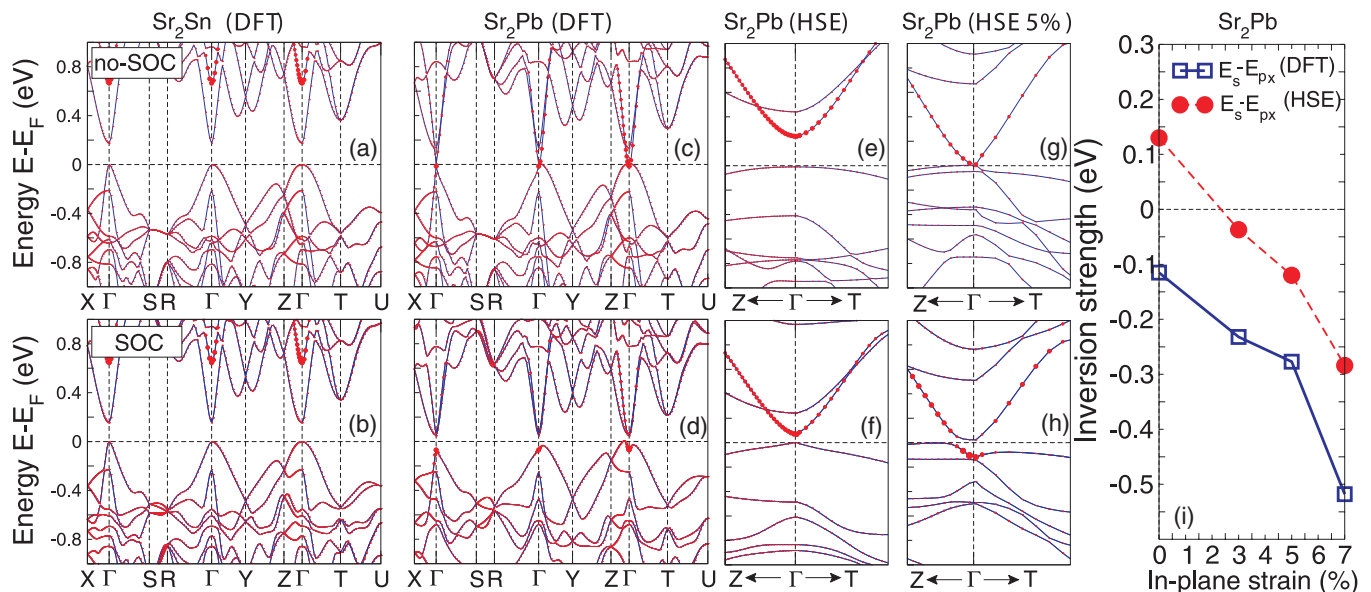


FIG. 2. (Color online) DFT and HSE electronic structure and band-inversion strength. DFT-calculated electronic band structures for (a,b) Sr_2Sn and (c,d) Sr_2Pb . HSE band structures around the Γ point along the Z - Γ - T directions for Sr_2Pb (e,f) at zero strain and (g,h) under 5% tensile strain in the ac plane. Results are calculated (a,c,e,g) without and (b,d,f,h) with SOC. The solid (red) circles denote the states with a predominant s -like character. (i) Comparison of the band-inversion strength between p_x and s orbitals at the Γ point as a function of strain. Negative values denote the occurrence of band inversion.

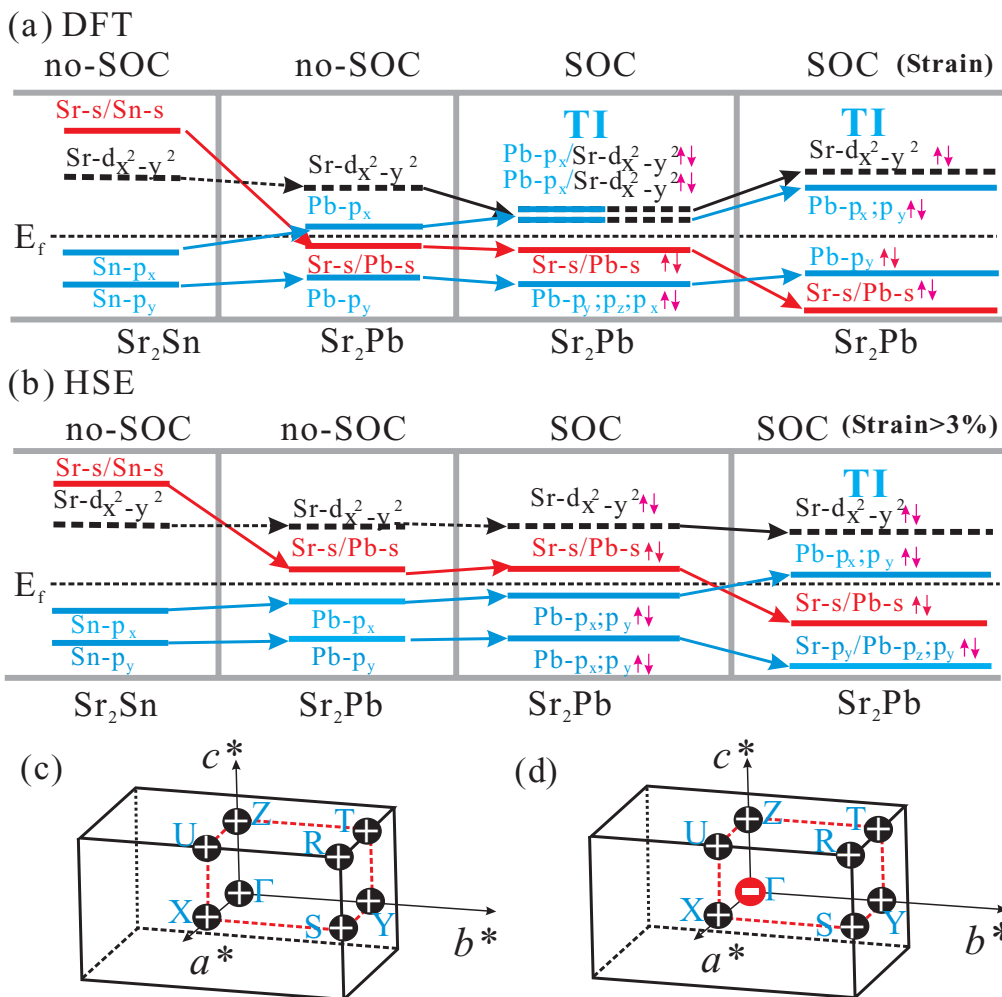


FIG. 3. (Color online) Evolution of atomic orbitals at the Γ point from Sr_2Sn to Sr_2Pb with and without SOC effects included for both (a) DFT and (b) HSE calculations. The band inversion can be observed by Pb (or Sr) s and Pb p_x orbitals. The product of wave function parities of the occupied bands for eight time-reversal invariant momenta (TRIM) in the Brillouin zone [Γ (0,0,0), X (π ,0,0), Y (0, π ,0), Z (0,0, π), S (π , π ,0), T (0, π , π), U (π ,0, π), and R (π , π , π)] of Sr_2Pb is obtained (c) before and (d) after band inversion, respectively.

s states remain well localized on the bottom of the conduction band [Figs. 2(e) and 2(f)]: Sr_2Pb is not a TI in its native phase. DFT wrongly stabilizes a spurious TI solution because of the relatively small band-inversion strength [0.12 eV; see Fig. 2(a)]. Though HSE is expected to provide a generally more accurate description of band dispersion in small-band-gap insulators, future optical experiments are necessary in order to validate our first-principles findings.

To explore possible routes for designing a TI phase in the native phase of Sr_2Pb , we carried out a series of calculations applying strain, a gap-engineering technique which was successful when applied to zero-gap semiconductors such as ternary Heusler compounds²² and Ca_3Nbi .²⁶ We have chosen to study the effect of uniaxial strain (ϵ) in the ac plane by leaving the b axis unconstrained (free to relax) in order to simulate best the experimental condition for thin-film growth. The results, obtained by HSE and shown in Figs. 2(g) and 2(h), indicate that for relatively small uniaxial strain larger than 3% Sr_2Pb can be tuned toward a TI phase. The role of SOC effects is essential to open a small gap around Γ and to induce an inverted band order. The s -like states shift downward below

the Fermi level and become occupied and, simultaneously, the p_x -like states become unoccupied and promoted at higher energy. This kind of inverted band behavior can be ascribed to the fact that the strain-induced expansion in the ac plane reduces the crystal field effect, resulting in less hybridization between s - and p -like states and stabilizing the s -like state at lower energy, as evidenced in Figs. 2(e) and 2(g). In such a way, the spin-orbit coupling strength is now enough to invert the band order between s -like and p -like states at Γ [c.f. Figs. 2(f) and 2(h)]. For larger strains up to 7% the TI state is preserved and further stabilized as inferred by the evolution of the band-inversion strength as a function of strain reported in Fig. 2(i) at both DFT and HSE levels.

In addition to the band inversion, an alternative way to identify TI states is the parity criteria proposed by Fu and Kane.¹⁰ Considering that orthorhombic $Pnma$ possesses the inversion symmetry, this criteria can be applied and serves as a further support for our analysis. The product of the parities of the Bloch wave function for the occupied bands at all eight time-reversal invariant momenta (TRIM), illustrated in Figs. 3(c) and 3(d), suggest that at six TRIMs (X, Y, Z, S, T,

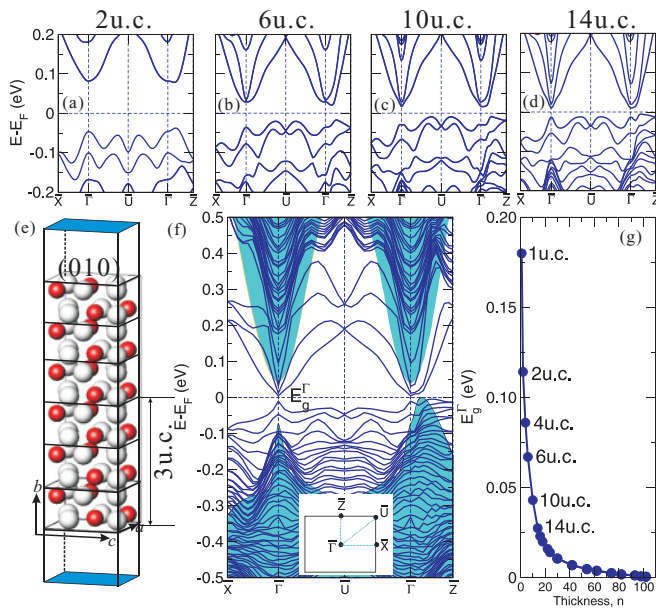


FIG. 4. (Color online) DFT surface properties of strained $\text{Sr}_2\text{Pb}(010)$ ($\epsilon = 5\%$). (a–d) Evolution of the band structures with slab thickness. (e) Structural model of the symmetric slab adopted to simulate the $\text{Sr}_2\text{Pb}(010)$ surface. (The image corresponds to the 3 unit-cell case, i.e., six layers per side. We adopted a vacuum region of 30 Å.) (f) Band structure for a thickness of 22 u.c. Shaded areas refer to bulk bands. (g) Progressive closing of the gap at Γ (E_g^Γ) as a function of the slab thickness. Note that, due to the prohibitive computational cost, for slab thickness larger than 34 u.c. (>400 atoms) the band gaps were calculated at Γ only.

and U) all bands share the same doubly degenerate character, whereas the TRIM R is found to be fourfold degenerate. Therefore all these seven TRIMs display a positive (+) global parity. At Γ the situation is different: the product of the parities is + or – depending on whether or not the band inversion occurs, consistent with the HSE band-structure interpretation [Figs. 3(c) and 3(d)]. We can therefore trustfully conclude that distorted orthorhombic Sr_2Pb is a topological nontrivial insulator with \mathbb{Z}_2 index (1; 000). Strain-driven gap engineering on Sr_2Sn does not result in any topological transition: Sr_2Sn remains a conventional semiconductor.

After discussing the onset of topological features in the bulk phase of distorted Sr_2Pb we turn our attention to the surface properties, focusing on the nonpolar (010) termination. Considering that both DFT and HSE lead to an essentially identical TI state in strained Sr_2Pb and that SOC-HSE calculations for thick slabs are computationally very demanding (if not prohibitive at all), we study the surface band structure at the DFT level only. The results on the $\text{Sr}_2\text{Pb}(010)$ surface are

summarized in Fig. 4, which shows that very thick slabs have topologically protected surface metallic states which remain robust with increasing film thickness, thus corroborating the conclusion of the bulk parity analysis and the inverted band order. The evolution of the band structure as a function of the film thickness shows a very peculiar behavior. Already at low film thickness surface-related states emerge in a small energy window (± 200 meV) around the Fermi level. This leads to a quenching of the band gap as compared to the bulk value (130 meV). The band gap is then progressively reduced by increasing the slab thickness. Although for a thickness of 22 u.c. [Fig. 4(f)] the gap is almost completely suppressed (10 meV), it is necessary to increase the thickness up to 100 u.c. in order to fabricate a well-defined metallic film [Fig. 4(g)]. At the critical thickness of 100 u.c., the lowest conduction band and the highest valence band meet at the Fermi level at Γ and establish a single-Dirac-cone-like metallic surface state.

IV. CONCLUSION

In conclusion, our computational study has disclosed the nontrivial topological nature of the binary compound Sr_2Pb , which is induced by small uniaxial strain. From the methodological point of view we have shown that PBE and HSE convey a fundamentally different picture when applied to the native (unstrained) phase of Sr_2Pb . The false-positive TI assignment delivered by PBE should be attributed to the underestimation of the band gap at this level of theory, which ultimately leads to a spurious SOC-driven band inversion at the critical point Γ .

The detailed analysis of the bulk and surface structural and electronic properties is of relevance for the design principles of TIs and provides helpful insight for tunability of TI states in trivial insulators by gap-engineering techniques. We believe that our findings will encourage immediate experimental investigations.

ACKNOWLEDGMENTS

The authors are grateful for support from the “Hundred Talents Project” of the Chinese Academy of Sciences and from the project of the NSFC of China (Grant Nos. 51074151, 51174188, and 51050110444) as well as the Supercomputing Center of the Chinese Academy of Sciences (including the Shenyang branch) and a local HPC cluster in the Materials Process Simulation Division, IMR, of CAS as well as the Vienna Scientific Cluster (VSC) in Austria. F.Z. acknowledges the support from the 973 program of China (Grant No. 2007CB925000).

*Corresponding author: xingqiu.chen@imr.ac.cn

¹M. Z. Hasan and C. L. Kane, *Rev. Mod. Phys.* **82**, 3045 (2010).

²J. E. Moore, *Nature (London)* **464**, 194 (2010).

³S.-C. Zhang, *Physics* **1**, 6 (2008).

⁴D. Hsieh, Y. Xia, L. Wray, D. Qian, A. Pal, J. H. Dil, F. Meier, J. Osterwalder, C. L. Kane, G. Bihlmayer, Y. S. Hor, R. J. Cava, and M. Z. Hasan, *Science* **323**, 5916 (2009).

⁵D. Hsieh, D. Qian, L. Wray, Y. Xia, Y. S. Hor, R. J. Cava, and M. Z. Hasan, *Nature (London)* **452**, 970 (2008).

- ⁶Y. Xia, D. Qian, D. Hsieh, L. Wray, A. Pal, H. Lin, A. Bansil, D. Grauer, Y. S. Hor, R. J. Cava, and M. Z. Hasan, *Nat. Phys.* **5**, 398 (2009).
- ⁷B. A. Bernevig, T. L. Tughes, and S.-C. Zhang, *Science* **314**, 1757 (2006).
- ⁸M. König, S. Wiedmann, C. Brüne, A. Roth, H. Buhmann, L. Molenkamp, X.-L. Qi, and S.-C. Zhang, *Science* **318**, 766 (2007).
- ⁹Y. L. Chen, J. G. Analytis, J.-H. Chu, Z. K. Liu, S.-K. Mo, X.-L. Qi, H. J. Zhang, D. H. Lu, X. Dai, Z. Fang, and S.-C. Zhang, *Science* **325**, 178 (2009).
- ¹⁰L. Fu and C. L. Kane, *Phys. Rev. B* **76**, 045302 (2007).
- ¹¹D. Hsieh, J. W. McIver, D. H. Torchinsky, D. R. Gardner, Y. S. Lee, and N. Gedik, *Phys. Rev. Lett.* **106**, 057401 (2011).
- ¹²Y. Xia, D. Qian, L. Wray, D. Hsieh, G. F. Chen, J. L. Luo, N. L. Wang, and M. Z. Hasan, *Phys. Rev. Lett.* **103**, 037002 (2009).
- ¹³H. J. Zhang, C.-X. Liu, X.-L. Qi, X. Dai, Z. Fang, and S.-C. Zhang, *Nat. Phys.* **5**, 438 (2009).
- ¹⁴B. Yan, C.-X. Liu, H.-J. Zhang, C.-Y. Yam, X.-L. Qi, T. Frauenheim, and S.-C. Zhang, *Europhys. Lett.* **90**, 37002 (2010).
- ¹⁵Y. L. Chen, Z. K. Liu, J. G. Analytis, J.-H. Chu, H. J. Zhang, B. H. Yan, S.-K. Mo, R. G. Moore, D. H. Lu, I. R. Fisher, S. C. Zhang Z. Hussain, and Z.-X. Shen, *Phys. Rev. Lett.* **105**, 266401 (2010).
- ¹⁶T. Sato, K. Segawa, H. Guo, K. Sugawara, S. Souma, T. Takahashi, and Y. Ando, *Phys. Rev. Lett.* **105**, 136802 (2010).
- ¹⁷S.-Y. Xu, L. A. Wray, Y. Xia, R. Shankar, A. Petersen, A. Fedorov, H. Lin, A. Bansil, Y. S. Hor, D. Grauer, R. J. Cava, and M. Z. Hasan, e-print [arXiv:1007.5111](https://arxiv.org/abs/1007.5111) (unpublished).
- ¹⁸H. Jin, J.-H. Song, A. J. Freeman, and M. G. Kanatzidis, *Phys. Rev. B* **83**, 041202(R) (2011).
- ¹⁹B. H. Yan, H.-J. Zhang, C.-X. Liu, X.-L. Qi, T. Frauenheim, and S.-C. Zhang, *Phys. Rev. B* **82**, 161108(R) (2010).
- ²⁰H.-J. Zhang, S. Chadov, L. Muchler, B. Yan, X.-L. Qi, J. Kübler, S.-C. Zhang, and C. Felser, *Phys. Rev. Lett.* **106**, 156402 (2011).
- ²¹H. Lin, L. A. Wray, Y. Xia, S. Xu, S. Jia, R. J. Cava, A. Bansil, and M. Z. Hasan, *Nat. Mater.* **9**, 546 (2010).
- ²²S. Chadov, X. L. Qi, J. Kübler, G. H. Fecher, C. Felser, and S. C. Zhang, *Nat. Mater.* **9**, 541 (2010).
- ²³D. Xiao, Y. Y. Yao, W. Feng, J. Wen, W. Zhu, X.-Q. Chen, G. M. Stocks, and Z. Zhang, *Phys. Rev. Lett.* **105**, 096404 (2010).
- ²⁴M. Klintonberg, e-print [arXiv:1007.4838](https://arxiv.org/abs/1007.4838) (unpublished).
- ²⁵W. Feng, D. Xiao, J. Ding, and Y. Yao, *Phys. Rev. Lett.* **106**, 016402 (2011).
- ²⁶Y. Sun, X.-Q. Chen, S. Yunoki, D. Z. Li, and Y. Y. Li, *Phys. Rev. Lett.* **105**, 216406 (2010).
- ²⁷W. Zhang, R. Yu, W. Feng, Y. Yao, H. Weng, X. Dai, and Z. Fang, *Phys. Rev. Lett.* **106**, 156808 (2011).
- ²⁸G. Bruzzone and E. Franceschi, *J. Less-Common Met.* **57**, 201 (1978).
- ²⁹P. Eckerlin and E. Wolfel, *Z. Anorg. Chem.* **280**, 321 (1955).
- ³⁰J. P. Perdew, K. Burke, and M. Ernzerhof, *Phys. Rev. Lett.* **77**, 3865 (1996).
- ³¹J. Heyd, G. E. Scuseria, and M. Ernzerhof, *J. Chem. Phys.* **118**, 8207 (2003); **124**, 219906 (2006).
- ³²G. Kresse and J. Hafner, *Phys. Rev. B* **48**, 13115 (1993).
- ³³G. Kresse and J. Furthmüller, *Comput. Mater. Sci.* **6**, 15 (1996).
- ³⁴J. Vidal, X. Zhang, L. Yu, J.-W. Luo, and A. Zunger, *Phys. Rev. B* **84**, 041109(R) (2011).